IEEE Access
Multidisciplinary | Rapid Review | Open Access Journal

Received June 15, 2020, accepted June 27, 2020, date of publication July 7, 2020, date of current version July 22, 2020.

Digital Object Identifier 10.1109/ACCESS.2020.3007627

Dual Cost Function Model Predictive Direct Speed Control With Duty Ratio Optimization for PMSM Drives

MING LIU[1,2], JIEFENG HU[3], (Senior Member, IEEE), KA WING CHAN[1], (Member, IEEE), SIU WING OR[1,2], SIU LAU HO[1,2], WENZHENG XU[1,2], AND XIAN ZHANG[1], (Member, IEEE)

[1]Department of Electrical Engineering, The Hong Kong Polytechnic University, Hong Kong
[2]Hong Kong Branch, National Rail Transit Electrification and Automation Engineering Technology Research Center, Hong Kong
[3]School of Engineering, Information Technology and Physical Sciences, Federation University Australia, Ballarat, VIC 3353, Australia

Corresponding author: Siu Wing Or (eeswor@polyu.edu.hk)

This work was supported in part by the Research Grants Council of the Hong Kong Special Administrative Region (HKSAR) Government under Grant R5020-18, and in part by the Innovation and Technology Commission of the HKSAR Government to the Hong Kong Branch of National Rail Transit Electrification and Automation Engineering Technology Research Center under Grant K-BBY1.

ABSTRACT Traditional speed control of permanent magnet synchronous motors (PMSMs) includes a cascaded speed loop with proportional-integral (PI) regulators. The output of this outer speed loop, i.e. electromagnetic torque reference, is in turn fed to either the inner current controller or the direct torque controller. This cascaded control structure leads to relatively slow dynamic response, and more importantly, larger speed ripples. This paper presents a new dual cost function model predictive direct speed control (DCF-MPDSC) with duty ratio optimization for PMSM drives. By employing accurate system status prediction, optimized duty ratios between one zero voltage vector and one active voltage vector are firstly deduced based on the deadbeat criterion. Then, two separate cost functions are formulated sequentially to refine the combinations of voltage vectors, which provide two-degree-of-freedom control capability. Specifically, the first cost function results in better dynamic response, while the second one contributes to speed ripple reduction and steady-state offset elimination. The proposed control strategy has been validated by both Simulink simulation and hardware-in-the-loop (HIL) experiment. Compared to existing control methods, the proposed DCF-MPDSC can reach the speed reference rapidly with very small speed ripple and offset.

INDEX TERMS Model predictive control, direct speed control, hardware-in-the-loop, permanent magnet synchronous machine.

I. INTRODUCTION

Due to the merits of high power density, high efficiency, etc., permanent magnet synchronous motors (PMSMs) have been widely used in electric drives. For a large variety of applications, suitable control schemes are highly desired to meet different operating conditions for PMSM drives. Researches on advanced control technologies, such as neural network control [1], fuzzy control [2], [3] and model predictive control (MPC), are emerging in recent years. MPC, which was initially designed to control the power converters [4], has attracted significant attention worldwide. Two popular research orientations are grid-connected converters [5]–[7] and machine drives [5], [31].

Intrinsically, MPC is capable of handling different control objectives with nonlinearity, multiple constraints and multiple variables. Based on the system mathematical model, future variations of system status can be predicted. Through the optimization by a well-defined cost function, optimal voltage vectors can be determined and applied to control PMSMs. Various MPC-based methods have been reported in recent years, like model predictive torque control (MPTC) [8]–[10], model predictive current control (MPCC) [11], [12] and model predictive flux control (MPFC) [13], [14]. The underlying control principles of different MPC strategies are similar, but with various cost functions.

The associate editor coordinating the review of this manuscript and approving it for publication was Bohui Wang.

Most existing MPC methods consist of a cascaded speed-to-torque loop [15]–[17] or speed-to-current loop [18]–[20], where a proportional-integral (PI) is usually included as a linear adapter. However, as PMSM system is a typical nonlinear system, MPC with PI controllers may result in a compromised control performance. Specifically, unsuitable PI parameters in speed loop would contribute to inferior control performance, such as large speed offset, high ripples of speed and torque. Complicated and time-consuming tuning methods are therefore required to achieve satisfactory performance.

Recently, to further enhance the control performance of MPC, improved control methods have been developed. A simple but effective method to enhance the control performance is to employ duty ratio modulation (DRM) method, where a zero voltage vector will be used together with a selected active voltage vector in one sampling period. When more than one voltage vector is applied in one sampling period, it is crucial to select an appropriate duty ratio; otherwise, the system performance will be compromised. Several methods have been proposed to determine the duty ratio such as deadbeat control [21]–[24]. Nevertheless, the duty ratio is calculated by the deadbeat criterion after the selection of the optimal voltage vector. The duty ratio may not be the optimal one after such step-by-step calculation. Improved approaches are still required to achieve the maximum benefit of DRM.

Another critical concern in MPC is the cost function. Usually, there is only one cost function in existing MPC methods, which is integrated by a few control variables, e.g., toque and flux for model predictive torque control (MPTC) [25], [26]. The weighting factor is inevitably involved to balance different control variables. The calculation of the weighting factor is a challenge that increases the complicity of MPC. To address this issue, an MPC method in [27] uses one cost function for the torque and a separate cost function for the flux, and a very fast dynamic behavior is achieved. However, although two cost functions are involved, there is only one voltage vector applied in a control period, and the torque ripple is still large.

More recently, by combining the advantages of MPC and direct speed control, model predictive direct speed control (MPDSC) is of great interest to realize an excellent speed control performance with satisfactory torque response. To authors' best knowledge, all existing MPDSC methods use only one voltage vector and one cost function in a sampling period, and the speed ripple and torque ripple are still requiring further optimization [28]–[31]. Moreover, parameter variations and measurement error effects would deteriorate the control performance in a practical control system. To deal with the adverse effect of these disturbances, observers are introduced to estimate various disturbances, and an enhanced control algorithm with disturbance compensations can be developed accordingly [32], [33]. It has been proven that the employment of observers contributes to develop a robust controller [34].

The main contributions of this paper are follows.

1) A PI-free dual cost function model predictive direct speed control (DCF-MPDSC) strategy with duty ratio modulation (DRM) is designed for PMSMs.

2) An on-line minimum order load torque observer (MOLTO) [35] is introduced to estimate load torque and enhance the robustness.

3) To make full use of DRM, duty ratios for eight voltage vectors are derived before the selection of acting voltage vector, based on the criterion of deadbeat speed control, to form eight combinations of voltage vectors.

4) The optimal combination of voltage vectors is selected using two cascaded cost functions acting sequentially.

The advantages of the proposed DCF-MPDSC strategy include fast dynamic response, speed and torque ripple reduction, and speed offset elimination. The rest of this paper is organized as follows. In Section II, the PMSM mathematical model is introduced. In Section III, a load torque observer is first developed for the estimation of load torque, and the motor behavior is predicted. In Section IV, the procedures to deduce eight duty ratios are introduced, and two cost functions are formulated to refine the combinations of voltage vectors. Section V and VI present simulation results and experimental tests, respectively.

II. PMSM MATHEMATICAL MODEL

PMSM mathematical model in dq reference frame is commonly employed due to its convenience on formula derivation. Based on the measured machine information, stator voltages and stator currents in dq synchronous coordinate can be obtained through the coordinate transformation. Following the well-known PMSM mathematical model [36], the differential equations of stator current are known as

$$\frac{di_d}{dt} = \frac{1}{L_d}\left(-R_s i_d + \varphi_q \omega + u_d\right) \tag{1}$$

$$\frac{di_q}{dt} = \frac{1}{L_q}\left(-R_s i_q - \varphi_d \omega + u_q\right) \tag{2}$$

where i_d and i_q are stator current in d- and q-axis respectively, L_d and L_q are the stator inductance in d- and q-axis respectively, R_s is the stator resistance, φ_d and φ_q are the stator flux in d- and q-axis respectively, u_d and u_q are stator voltage in d- and q-axis respectively, and ω is the rotor speed.

The mathematical expression of stator flux $\boldsymbol{\varphi}$ is

$$\boldsymbol{\varphi} = \varphi_d + j\varphi_q = \left(L_d i_d + \varphi_f\right) + j\left(L_q i_q\right) \tag{3}$$

where φ_f is the permanent magnet flux. The derivative of stator flux is obtained as

$$\frac{d\left|\boldsymbol{\varphi}\right|}{dt} = \frac{L_d \varphi_d \frac{di_d}{dt} + L_q \varphi_q \frac{di_q}{dt}}{\sqrt{\varphi_d^2 + \varphi_q^2}} \tag{4}$$

After the mathematical manipulation of Eq. (1)-(3), the stator voltages $\boldsymbol{u}_s$ can be expressed as

$$\begin{aligned}\boldsymbol{u}_s &= u_d + j u_q \\ &= \left(R_s i_d + \frac{d\varphi_d}{dt} - \omega\varphi_q\right) + j\left(R_s i_q + \frac{d\varphi_q}{dt} + \omega\varphi_d\right)\end{aligned} \tag{5}$$

The electromagnetic torque T can be obtained as

$$T = 1.5p\left(\varphi_d i_q - \varphi_q i_d\right) = 1.5p\left(\varphi_f i_q + \Delta L i_d i_q\right) \quad (6)$$

where p is the number of pole pairs, and $\Delta L = L_d - L_q$. The first-order differential of electromagnetic torque T with respect to time t can be obtained as

$$s_T = \frac{dT}{dt} = 1.5p\left(\varphi_f \frac{di_q}{dt} + \Delta L\left(\frac{di_d}{dt} i_q + i_d \frac{di_q}{dt}\right)\right) \quad (7)$$

The mechanical equation of PMSMs can be expressed as

$$s_\omega = \frac{d\omega}{dt} = \frac{1}{J}\left(T - B_m\omega - T_L\right) \quad (8)$$

where J is the moment of inertia, B_m is the vicious friction, and T_L is the load torque. Equations (7) and (8) present the mathematical expressions to calculate the slope of torque s_T and the slope of rotor speed s_ω respectively, which will be employed in the proposed system status prediction.

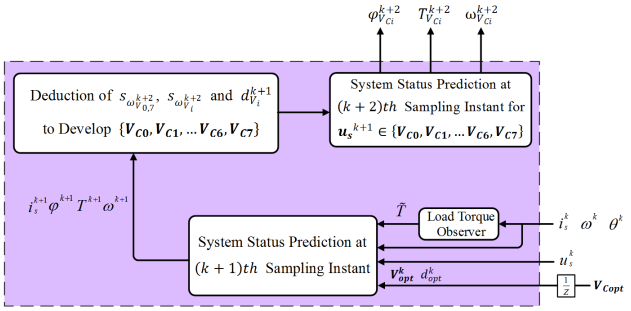

FIGURE 1. System status prediction.

III. MOTOR BEHAVIOR PREDICTION

In predictive direct speed control, the key is to predict the rotor speed ω accurately so that proper control set can be applied. Fig. 1 illustrates the system status prediction, including a load torque observer, system status prediction and duty ratio optimization. After the machine information is collected at the k^{th} sampling instant, control code will be executed during the k^{th} sampling period to output suitable voltage vectors to control the motor at the $(k+1)^{th}$ sampling instant. In other words, one-step delay is unavoidable due to the characteristics of practical controllers. It is thus advantageous to compensate the one-step delay by incorporating the system status prediction at $(k+2)^{th}$ sampling instant.

A. LOAD TORQUE OBSERVER

In motor drives, torque sensors, or torque transducers, are needed to obtain actual torque information. Such devices, however, are usually expensive and hence, increase the system cost. Here, an on-line minimum order load torque observer (MOLTO) [35] is employed to predict the load torque in real-time. Such MOLTO system is defined as

$$\begin{bmatrix}\dot{x}_a \\ \dot{x}_b\end{bmatrix} = \begin{bmatrix}A_{aa} & A_{ab} \\ A_{ba} & A_{bb}\end{bmatrix}\begin{bmatrix}x_a \\ x_b\end{bmatrix} + \begin{bmatrix}B_a \\ B_b\end{bmatrix} u \quad (9)$$

$$\mathrm{y} = \begin{bmatrix}C_a & C_b\end{bmatrix}\begin{bmatrix}x_a \\ x_b\end{bmatrix} \quad (10)$$

where

$$\boldsymbol{x} = \begin{bmatrix}T_L & \omega\end{bmatrix}^T, \quad u = T,$$
$$\mathbf{A} = \begin{bmatrix}0 & 0 \\ -\frac{1}{J} & -\frac{B_m}{J}\end{bmatrix}, \quad \mathbf{B} = \begin{bmatrix}0 \\ \frac{1}{J}\end{bmatrix}, \ \mathbf{C} = \begin{bmatrix}0 & 1\end{bmatrix}. \quad (11)$$

T_L and ω are selected as the state variables. As T_L changes slowly with time during a short sampling period, it is assumed that $\dot{T}_L = 0$. The state variable ω can be directly measured, and is equal to the output y. According to (9) and (10), the estimated load torque $\tilde{T}_L$ can be expressed as

$$\tilde{T}_L = \tilde{z} + vJ\omega \quad (12)$$

$$\dot{\tilde{z}} = \frac{K_e}{J}\left(\tilde{z} + vJ\omega + B_m\omega - T\right) \quad (13)$$

where K_e is the observer gain, and v is the observer desired pole. The value of $\tilde{z}$ in (12) can be calculated using (13) with the initial condition $\tilde{z}_{t=0} = 0$. Based on the pole assignment guidelines, a negative value of v should be assigned to guarantee the stability of MOLTO.

B. SYSTEM STATUS PREDICTION AT $(k+1)^{th}$ SAMPLING INSTANT

There are totally eight voltage vectors that can be applied, i.e., $\boldsymbol{u_s} \in \{\boldsymbol{V_0}, \boldsymbol{V_1}, \ldots \boldsymbol{V_6}, \boldsymbol{V_7}\}$. To predict the system status at $(k+1)^{th}$ sampling instant, the differential equations of stator current for nonzero voltage vector (one of $\{\boldsymbol{V_1}, \boldsymbol{V_2}, \ldots \boldsymbol{V_6}\}$) and zero voltage vectors ($\boldsymbol{V_0}$ or $\boldsymbol{V_7}$) should be derived in advance. When the nonzero voltage vector is applied during the control period, (1) and (2) can be rewritten as

$$\frac{di_{d\_V_i}^k}{dt} = \frac{1}{L_d}\left(-R_s i_d^k + \varphi_q^k\omega^k + u_d^k\right) \quad (14)$$

$$\frac{di_{q\_V_i}^k}{dt} = \frac{1}{L_q}\left(-R_s i_q^k - \varphi_d^k\omega^k + u_q^k\right) \quad (15)$$

Similarly, when zero voltage vectors are selected and applied during the control period, (1) and (2) can be rewritten as

$$\frac{di_{d\_V_{0,7}}^k}{dt} = \frac{1}{L_d}\left(-R_s i_d^k + \varphi_q^k\omega^k\right) \quad (16)$$

$$\frac{di_{q\_V_{0,7}}^k}{dt} = \frac{1}{L_q}\left(-R_s i_q^k - \varphi_d^k\omega^k\right) \quad (17)$$

In the proposed DCF-MPDSC strategy, the optimal combination of voltage vectors, named $\boldsymbol{V_{Copt}}$, will be selected and applied to control the PMSM. $\boldsymbol{V_{Copt}}$ consists of one voltage vector $\boldsymbol{V_{opt}}$, i.e., one of $\{\boldsymbol{V_0}, \boldsymbol{V_1}, \ldots \boldsymbol{V_6}, \boldsymbol{V_7}\}$, and its corresponding duty ratio d_{opt} based on deadbeat speed criterion. At $(k-1)^{th}$ sampling instant, an optimal combination of voltage vectors $\boldsymbol{V_{Copt}^k}$, consisting of $\boldsymbol{V_{opt}^k}$ and d_{opt}^k, has been selected to be applied to the two-level three-phase inverter during the control period from k^{th} sampling instant to $(k+1)^{th}$ sampling instant. The selection process of $\boldsymbol{V_{Copt}^k}$ will be presented in the following sections.

At k^{th} sampling instant, with the measured machine information at k^{th} sampling instant, including $\boldsymbol{i}_s^k$, $\boldsymbol{u}_s^k$, ω^k and θ^k, and the $\boldsymbol{V}_{\boldsymbol{Copt}}^{\boldsymbol{k}}$ determined at $(k-1)^{th}$ sampling instant, the stator currents at $(k+1)^{th}$ sampling instant are calculated as

$$i_d^{k+1} = i_d^k + d_{opt}^k T_s \frac{di_{d\_V_i}^k}{dt} + \left(1 - d_{opt}^k\right) T_s \frac{di_{d\_V_{0,7}}^k}{dt} \tag{18}$$

$$i_q^{k+1} = i_q^k + d_{opt}^k T_s \frac{di_{q\_V_i}^k}{dt} + \left(1 - d_{opt}^k\right) T_s \frac{di_{q\_V_{0,7}}^k}{dt} \tag{19}$$

where T_s is the sampling period. Meanwhile, the electromagnetic torque T^{k+1} at $(k+1)^{th}$ sampling instant can be derived by equation (6). The speed at $(k+1)^{th}$ sampling instant is thus obtained using (8).

$$\omega^{k+1} = \omega^k + \frac{T_s}{J}\left(T^{k+1} - \tilde{T}_L - B_m\omega^k\right) \tag{20}$$

C. EFFECT OF ZERO VECTORS

With the obtained prediction model, the optimal duty ratio for speed control can now be determined. Usually, only one voltage vector is applied in each sampling period in traditional motor control. But, in fact, more than one vector, one zero vector and one active vector for example, can lead to better performance. Although this method has been adopted in direct torque control, so far it has not been studied in direct speed control yet due to the complicated speed prediction model. Now, before deriving the duty ratio for direct speed control, it is better to investigate into the effects of different voltage vectors on the PMSM. More specifically, for eight voltage vectors, $\frac{dT}{dt}$, $\frac{d\omega}{dt}$ and $\frac{d|\boldsymbol{\varphi}|}{dt}$ are investigated to present a clear analysis.

Based on the derived equations (4), (7) and (8), the variation of $\frac{d|\boldsymbol{\varphi}|}{dt}$, $\frac{dT}{dt}$ and $\frac{d\omega}{dt}$ are depicted for eight voltage vectors within the electric angle range from 0° to 360°, as shown in Fig. 2. Every particular electric angle corresponds to a specific sampling instant, and different voltage vectors result in various values of $\frac{dT}{dt}$, $\frac{d\omega}{dt}$ and $\frac{d|\boldsymbol{\varphi}|}{dt}$. Taking $\boldsymbol{V_1}$(red curve) for instance, when electric angle is 60°, $\frac{dT}{dt}$ and $\frac{d\omega}{dt}$ are positive values, which indicates that applying $\boldsymbol{V_1}$ can increase both the electromagnetic torque and rotor speed; however, $\frac{d|\boldsymbol{\varphi}|}{dt}$ is a negative value, resulting in a decreased stator flux by applying $\boldsymbol{V_1}$. Meanwhile, by applying zero voltage vectors ($\boldsymbol{V_0}$ or $\boldsymbol{V_7}$), $\frac{dT}{dt}$, $\frac{d\omega}{dt}$ and $\frac{d|\boldsymbol{\varphi}|}{dt}$ are all very small (almost zero), indicating that zero voltage vectors will not cause significant changes in the controlled variables. Consequently, with the insertion of the zero voltage vectors, the PMSM can be better controlled with reduced ripples in torque, speed or flux, provided that the duty ratio between the active vector duration and the zero vector duration can be optimized.

IV. PROPOSED DCF-MPDSC

A. EIGHT COMBINATIONS OF VOLTAGE VECTORS

After the investigation of zero vector effect, eight combinations of voltage vectors based on the deadbeat speed control would be developed. The predicted parameters at the

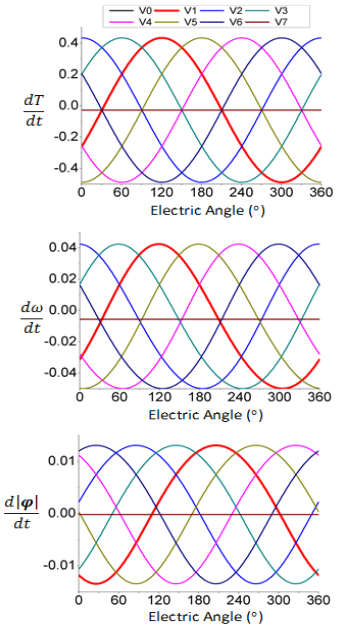

FIGURE 2. $\frac{dT}{dt}$, $\frac{d\omega}{dt}$ and $\frac{d|\varphi|}{dt}$ for eight voltage vectors.

$(k+1)^{th}$ sampling instant, along with eight voltage vectors $\boldsymbol{u}_s^{k+1} \in \{\boldsymbol{V_0}, \boldsymbol{V_1}, \ldots \boldsymbol{V_6}, \boldsymbol{V_7}\}$, will be employed in the following procedures to develop the combinations of voltage vectors.

When the zero voltage vector ($\boldsymbol{V_0}$ or $\boldsymbol{V_7}$) is applied to the two-level inverter during the whole period from $(k+1)^{th}$ to $(k+2)^{th}$ sampling instant, $\frac{di_{d\_V_{0,7}}^{k+1}}{dt}$ and $\frac{di_{q\_V_{0,7}}^{k+1}}{dt}$ can be obtained as

$$i_{d\_V_{0,7}}^{k+2} = i_d^{k+1} + T_s \frac{di_{d\_0,7}^{k+1}}{dt} \tag{21}$$

$$i_{q\_V_{0,7}}^{k+2} = i_q^{k+1} + T_s \frac{di_{q\_0,7}^{k+1}}{dt} \tag{22}$$

Following the deduction procedures presented before, the corresponding electromagnetic torque $T_{V_{0,7}}^{k+2}$ is thus derived by (6), which is further used to calculate the rotor speed at $(k+2)^{th}$ sampling instant

$$\omega_{V_{0,7}}^{k+2} = \omega^{k+1} + \frac{T_s}{J}\left(T_{0,7}^{k+2} - \tilde{T}_L - B_m\omega^{k+1}\right) \tag{23}$$

The speed slope $s_{\omega_{V_{0,7}}^{k+2}}$, which can reflect the effect of applied zero voltage vector ($\boldsymbol{V_0}$ or $\boldsymbol{V_7}$) during the whole period from $(k+1)^{th}$ to $(k+2)^{th}$ sampling instant, is therefore deduced as

$$s_{\omega_{V_{0,7}}^{k+2}} = \frac{d\omega_{V_{0,7}}^{k+2}}{dt} = \frac{1}{J}\left(T_{V_{0,7}}^{k+2} - T_L - B_m\omega_{V_{0,7}}^{k+2}\right) \tag{24}$$

Following the above steps (21)-(24), for eight voltage vectors $\boldsymbol{u}_s^{k+1} \in \{\boldsymbol{V_0}, \boldsymbol{V_1}, \ldots \boldsymbol{V_6}, \boldsymbol{V_7}\}$, the slope of speed $s_{\omega_{V_i}^{k+2}}(\mathrm{i} = 0, 1, \ldots 7)$, representing the speed changing tendency from $(k+1)^{th}$ to $(k+2)^{th}$ sampling instant, can be

obtained as

$$s_{\omega_{V_i}^{k+2}} = \frac{d\omega_{V_i}^{k+2}}{dt} = \frac{1}{J}\left(T_{V_i}^{k+2} - T_L - B_m\omega_{V_i}^{k+2}\right) \quad (25)$$

Based on the deadbeat speed criterion, the duty ratio for eight voltage vectors can be calculated as

$$d_{V_i}^{k+1} = \frac{\omega^* - \omega^{k+1} - T_s(s_{\omega_{V_{0,7}}^{k+2}})}{T_s(s_{\omega_{V_i}^{k+2}} - s_{\omega_{V_{0,7}}^{k+2}})} \quad (\mathrm{i} = 0, 1, \ldots 7) \quad (26)$$

It should be mentioned that the magnitude of $d_{V_i}^{k+1}$ is in the range of [0, 1]. The possible combination does not have to always contain one active voltage vector and one zero voltage vector. For example, $d_{V_i}^{k+1} = 0$ indicates only one zero voltage vector is applied during a control period.

Every voltage vector has its corresponding duty ratio $d_{V_i}^{k+1}$, which indicates that there are eight combinations of voltage vectors, as shown in Table 1. Each combination consists of an active voltage vector and a duty ratio based on the deadbeat speed criterion. With the consideration of the reduction of switching frequency, the corresponding zero voltage vectors are inserted properly, as tabulated in Table 2.

TABLE 1. Eight combinations of voltage vectors.

Combination of Voltage Vectors	Active Voltage Vector	Duty Ratio Based on Deadbeat Speed Criterion
$\boldsymbol{V_{C0}}$	$\boldsymbol{V_0}$=**0**	$d_{V_0}^{k+1} = 0$
$\boldsymbol{V_{C1}}$	$\boldsymbol{V_1}$	$d_{V_1}^{k+1}$
$\boldsymbol{V_{C2}}$	$\boldsymbol{V_2}$	$d_{V_2}^{k+1}$
$\boldsymbol{V_{C3}}$	$\boldsymbol{V_3}$	$d_{V_3}^{k+1}$
$\boldsymbol{V_{C4}}$	$\boldsymbol{V_4}$	$d_{V_4}^{k+1}$
$\boldsymbol{V_{C5}}$	$\boldsymbol{V_5}$	$d_{V_5}^{k+1}$
$\boldsymbol{V_{C6}}$	$\boldsymbol{V_6}$	$d_{V_6}^{k+1}$
$\boldsymbol{V_{C7}}$	$\boldsymbol{V_7}$=**0**	$d_{V_7}^{k+1} = 0$

TABLE 2. Zero vector arrangement to reduce switching frequency.

Combination of Voltage Vectors	Corresponding Zero Voltage Vectors to Minimize Switching Frequency
$\boldsymbol{V_{C0}}$	$\boldsymbol{V_0}$
$\boldsymbol{V_{C1}}$	$\boldsymbol{V_0}$
$\boldsymbol{V_{C2}}$	$\boldsymbol{V_0}$
$\boldsymbol{V_{C3}}$	$\boldsymbol{V_7}$
$\boldsymbol{V_{C4}}$	$\boldsymbol{V_0}$
$\boldsymbol{V_{C5}}$	$\boldsymbol{V_7}$
$\boldsymbol{V_{C6}}$	$\boldsymbol{V_7}$
$\boldsymbol{V_{C7}}$	$\boldsymbol{V_7}$

B. MULTIPART FIGURES SYSTEM STATUS PREDICTION AT $(k+2)^{th}$ SAMPLING INSTANT

One of eight combinations of voltage vectors will be selected and applied during the control period from $(k+1)^{th}$ sampling instant to $(k+2)^{th}$ sampling instant. The parameters at $(k+1)^{th}$ sampling instant are already obtained in Section II.B. Following the similar procedures from (14) to (20), the parameter estimation can be conducted once again for $(k+2)^{th}$ sampling instant for each of eight combinations of voltage vectors. Eight combinations of voltage vectors can deduce eight groups of parameters at $(k+2)^{th}$ sampling instant, and each group consists of the following parameters: the stator currents $i_{d\_V_{Ci}}^{k+2}$ and $i_{q\_V_{Ci}}^{k+2}$, stator fluxes $\varphi_{d\_V_{Ci}}^{k+2}$ and $\varphi_{q\_V_{Ci}}^{k+2}$, the electromagnetic torque $T_{V_{Ci}}^{k+2}$ and the rotor speed $\omega_{V_{Ci}}^{k+2}(\mathrm{i} = 0, 1, \ldots 7)$. Specifically, the stator flux can be deduced as

$$\boldsymbol{\varphi_{V_{Ci}}^{k+2}} = \varphi_{d\_V_{Ci}}^{k+2} + j\varphi_{q\_V_{Ci}}^{k+2} = \left(L_d i_{d\_V_{Ci}}^{k+2} + \varphi_f\right) + j\left(L_q i_{q\_V_{Ci}}^{k+2}\right) \quad (27)$$

the electromagnetic torque $T_{V_{Ci}}^{k+2}$ can be expressed as

$$T_{V_{Ci}}^{k+2} = 1.5p\left(\varphi_f i_{q\_V_{Ci}}^{k+2} + \Delta L i_{d\_V_{Ci}}^{k+2} i_{q\_V_{Ci}}^{k+2}\right) \quad (28)$$

and the rotor speed $\omega_{V_{Ci}}^{k+2}$ is

$$\omega_{V_{Ci}}^{k+2} = \omega^{k+1} + \frac{T_s}{J}\left(T_{V_{Ci}}^{k+2} - \tilde{T}_L - B_m\omega^{k+1}\right) \quad (29)$$

C. DUAL COST FUNCTION OPTIMIZATION

Now, two cost functions (g_1 and g_2) will be designed to finally determine the optimal voltage vector combination. Specifically, three pre-selected voltage vector sequences will be shortlisted by g_1. After that, the ultimate optimal voltage vector sequence will be determined by g_2.

The first cost function g_1 is defined as

$$\begin{aligned} &min.\ g_1 = C_1 + C_T \\ &\text{s.t. } \boldsymbol{u_s^{k+1}} \in \{\boldsymbol{V_{C0}}, \boldsymbol{V_{C1}}, \ldots \boldsymbol{V_{C6}}, \boldsymbol{V_{C7}}\} \end{aligned} \quad (30)$$

g_1 consists of two parts, i.e., C_1 and C_T. The objective of C_1 is to enhance the dynamic response, which is defined as

$$C_1 = \left|T_{V_{Ci}}^{k+2} - T_r\right| \quad (\mathrm{i} = 0, 1, \ldots 7) \quad (31)$$

where T_r is the torque reference. C_1 is to find the most powerful voltage vectors, and thus to enhance the dynamic response. However, there is no limitation on the predicted value of electromagnetic torque $T_{V_{Ci}}^{k+2}$. Thus, the electromagnetic torque could exceed the rated limit during transients, such as start-up, speed-up and speed-down. Such undesired overshoot of electromagnetic torque may damage the whole PMSM system. A compensation factor C_T is therefore introduced in the cost function g_1 to refine the selected voltage vectors.

$$C_T = \begin{cases} \infty & \left|T_{V_{Ci}}^{k+2}\right| > T_r \\ 0 & \left|T_{V_{Ci}}^{k+2}\right| \le T_r \end{cases} \quad (32)$$

The compensation factor C_T has two values, i.e. ∞ and 0. When $T_{V_{Ci}}^{k+2}$ is greater than the rated value, i.e. T_r, compensation factor C_T is equal to ∞. This means that the

corresponding voltage vector V_i will not be selected as it will cause large torque oscillations. In contrast, when $T_{V_{Ci}}^{k+2}$ is smaller than T_r, compensation factor C_T becomes 0, which indicates that the corresponding voltage vector V_i is of higher selection priority, and it could be selected provided it also leads to a small value of C_1.

At the first selection stage, three combinations of voltage vectors ($\boldsymbol{V_{Cs_1}}, \boldsymbol{V_{Cs_2}}, \boldsymbol{V_{Cs_3}}$) that can generate three smallest values of the cost function g_1 will be preselected, awaiting to be evaluated again at the second selection stage. Since three combinations of voltage vectors have been preselected by the first cost function g_1 to guarantee a good dynamic response, there is still selection freedom remaining for the second cost function g_2 to manipulate the speed and flux.

At the second selection stage, the second cost function g_2 is defined as

$$\begin{aligned} &min.\ g_2 = C_2 + C_T \\ &\text{s.t. } \boldsymbol{u_s}^{k+1} \in \left\{\boldsymbol{V_{Cs_1}}, \boldsymbol{V_{Cs_2}}, \boldsymbol{V_{Cs_3}}\right\} \end{aligned} \tag{33}$$

g_2 consists of two parts. The first part C_2 is defined as

$$C_2 = \left|\omega_{V_{Cs_i}}^{k+2} - \omega^*\right| + k\left|\varphi_{V_{Cs_i}}^{k+2} - \varphi^*\right| \quad (\mathrm{i} = 1, 2, 3) \tag{34}$$

where $\varphi_{V_{Cs_i}}^{k+2} = \sqrt{\left(\varphi_{d\_V_{Cs_i}}^{k+2}\right)^2 + \left(\varphi_{q\_V_{Cs_i}}^{k+2}\right)^2}$. A weighting factor k is introduced to balance the unit between speed and flux. In C_2, the first term aims to track the rotor speed reference and minimize the speed ripple. The stator flux is regulated by the second term in C_2. If the stator flux $\varphi_{V_{Cs_i}}^{k+2}$ can track the stator flux reference φ^*, smaller ripple of stator flux results in lower stator current's total harmonic distortion (THD), which contributes to more sinusoidal current waveform.

Once again, it is necessary to integrate C_T into g_2 to avoid the selection of undesired voltage vector combination. As three combinations of voltage vectors are forced to be preselected by the first cost function g_1, some of them may include the compensation factor C_T with ∞, and these combinations of voltage vectors should be excluded from the final selection. Without C_T in the second cost function g_2, undesired combination of voltage vector could be selected as the optimal one, which may damage the PMSM. Adding C_T can further enhance the stability of the proposed DCF-MPDSC. Consequently, with the refinement of cost function g_2, an optimal combination of voltage vectors $\boldsymbol{V_{Copt}^{k+1}}$ is finally selected and applied to the PMSM. The corresponding active voltage vector and duty ratio are $\boldsymbol{V_{opt}^{k+1}}$ and $d_{V_{opt}}^{k+1}$ respectively.

D. OVERALL CONTROL DIAGRAM

The overall control diagram of the proposed DCF-MPDSC strategy is illustrated in Fig. 3, and the control process is explained as follows.

Step 1. *System Status Prediction (as is depicted in Fig. 1)*

1) The load torque is first estimated using a load torque observer (12-13).

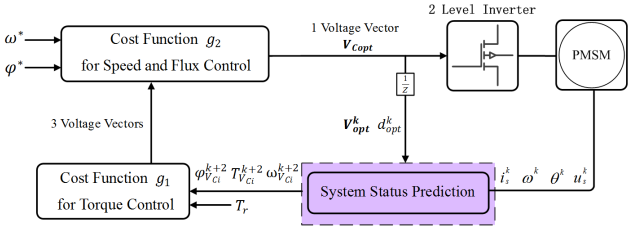

FIGURE 3. Block diagram of the overall proposed DCF-MPDSC strategy.

2) The estimated load torque $\tilde{T}_L$, together with real-time measurements from the PMSM and the optimal combination of voltage vectors $\boldsymbol{V_{Copt}}$ determined at $(k-1)^{th}$ sampling instant, will be used to conduct the system status prediction at $(k+1)^{th}$ sampling instant.
3) Then, eight duty ratios $d_{V_i}^{k+1}$ corresponding to eight possible voltage vectors V_i can be calculated using the slope of speed $s_{\omega_{V_i}^{k+2}}(\mathrm{i} = 0, 1, \ldots 7)$ according to the deadbeat speed criterion, as shown in (26). Eight combinations of voltage vectors are thus formed as shown in Table 1. The system status at $(k+2)^{th}$ sampling instant is predicted for every combination of voltage vectors by the procedures from (14) to (20).

Step 2. *Selecting optimal combination of voltage vectors* $\boldsymbol{V_{Copt}}$ *by dual cost function (as is depicted in Fig. 3)*

4) To select the optimal combination of voltage vectors $\boldsymbol{V_{Copt}}$, a cost function g_1 (30) is first used to pre-select three combinations of voltage vectors, i.e., $\boldsymbol{V_{Cs_1}}, \boldsymbol{V_{Cs_2}}, \boldsymbol{V_{Cs_3}}$, which can provide the most powerful capability on dynamic response enhancement.
5) The optimal combination of voltage vectors $\boldsymbol{V_{Copt}}$ out of three combinations of voltage vectors is then further determined by the second cost function g_2 (33) for speed and flux control. At this step, the optimal combination of voltage vectors $\boldsymbol{V_{Copt}}$ is saved in the register waiting to be applied to PMSM, as well as to be used to conduct system status prediction on next control period.

V. NUMERICAL SIMULATION

The proposed MPDSC strategy is validated by numerical simulation in MATLAB/Simulink in this section. Table 3 presents the PMSM system parameters. Under the same sampling frequency, various control methods result in different switching frequencies. To make a fair comparison, the same average switching frequencies are achieved by using different sampling frequencies for different control methods.

To demonstrate the effectiveness of the proposed strategy, different methods are compared. The conventional DTC with an outer speed-to-torque loop [37], [38] is served as a benchmark for the comparison. Conventional MPDSC uses one cost function to select one voltage vector. It will

TABLE 3. PMSM system data.

Symbol	Constants	Values
p	number of pole pairs	5
φ_f	PM rotor flux	0.088 Wb
R_s	stator resistance	0.636 Ω
L_d	d-axis inductance	0.012 H
L_q	q-axis inductance	0.02 H
B_m	viscous friction	0.0017 kgm/s^2
J	moment of inertia	0.001 kgm^2
T_r	rated torque	7.8 Nm
ω_r	rated speed	1000 rpm
I_r	rated current	11.36A
k	weighting factor	1
T_s	sampling time	100 µs
U_{DC}	DC bus voltage	200 V

be therefore compared with the proposed DCF-MPDSC with two cost functions and two voltage vectors. Further, to demonstrate the need of two cost functions, a single-cost function MPDSC (SCF-MPDSC) should be compared with the proposed DCF-MPDSC as well. As a result, the methods for comparison are carefully selected as follows.

Method 1 - Conventional direct torque control (DTC) [37], [38]

Method 2 - Conventional MPDSC [31]

Method 3 - Optimal duty ratio MPDSC with a single cost function g_2 (32), named as SCF-MPDSC

Method 4 - Optimal duty ratio MPDSC with cost functions g_1 (29) and g_2 (32), i.e., the proposed DCF-MPDSC

A. STEADY STATE RESPONSE

The steady-state responses of the conventional DTC, the conventional MPDSC, SCF-MPDSC and the proposed DCF-MPDSC are presented in Fig. 4. First, the conventional DTC shown in Fig. 4(a) exhibits the largest speed offset (1.3407%) and speed ripple (0.3619 rpm). Obviously, this is because the voltage vector is selected according to a pre-defined switching table. Such chosen voltage vector is not necessarily the optimal one to regulate the torque and speed. In Fig. 4 (b), conventional MPDSC presents a speed offset of about 0.0665% and speed ripple of 0.129 rpm, performing a slightly better result than DTC. This is as expected since the voltage vector is calculated in very sampling period according to a cost function rather than kept constant for a whole sector according to the switching table. Then, in Fig. 4(c), optimal duty ratio MPDSC is used but with only cost function g_2. It can be seen that the speed and torque performance are even worse than that of conventional MPDSC. On the other hand, by using the proposed optimal duty ratio DCF-MPDSC with two cost functions, the motor shows the best performance, as shown in Fig. 4(d). The speed offset and speed ripple of the proposed DCF-MPDSC are only 0.0051% and 0.0131 rpm respectively, which are absolutely excellent and encouraging. Meanwhile, compared to other methods, torque ripples have been reduced significantly as well with more sinusoidal stator currents. The comparison validates

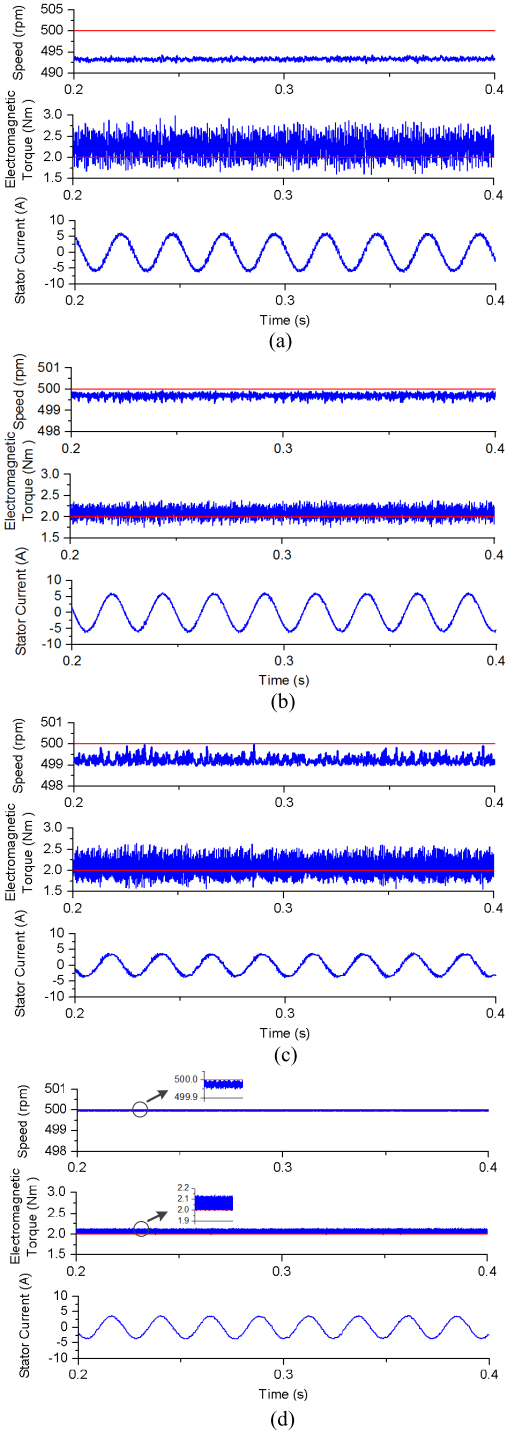

FIGURE 4. Comparisons of steady state response for various control methods when speed is 500 rpm: (a) the conventional DTC, (b) the conventional MPDSC, (c) SCF-MPDSC, (d) proposed DCF-MPDSC.

the effectiveness and superiority of the proposed DCF-MPDSC. In particular, the inferior steady state performance of SCF-MPDSC validates the necessity of the employment of two cost functions in the proposed DCF-MPDSC.

To give a more straightforward comparison among four control methods, the stator current THD, the torque ripple, the speed ripple, and the speed offset are summarized

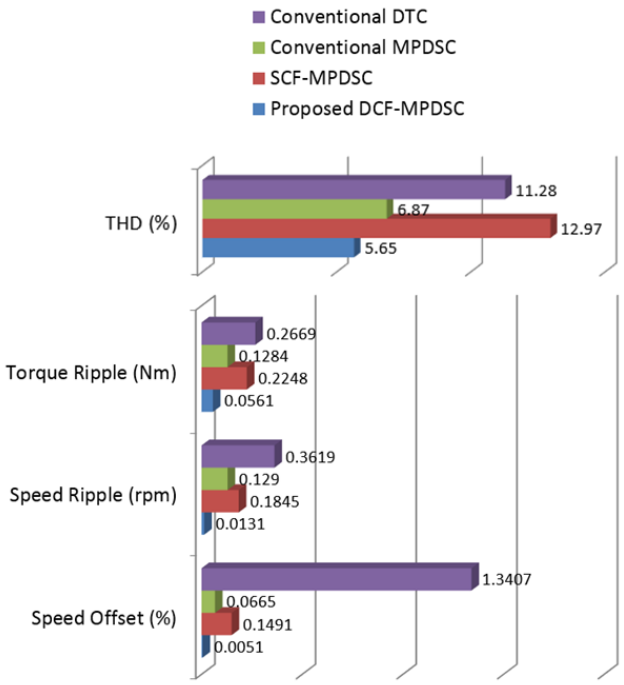

FIGURE 5. The comparison bar graph for (a) the conventional DTC, (b) the conventional MPDSC, (c) SCF-MPDSC, (d) proposed DCF-MPDSC.

in Fig. 5. It quantitatively demonstrates that the proposed DCF-MPDSC has significant improvement over existing methods with current THD, torque ripple, speed ripple, and speed offset at 4.43%, 0.0423Nm, 0.0121rpm and 0.0055%, respectively.

B. DYNAMIC RESPONSE

When the speed changes from 500 rpm to 1000 rpm at 0.3s, Fig. 6 shows the dynamic response of the conventional DTC, the conventional MPDSC, SCF-MPDSC and the proposed DCF-MPDSC, respectively. A common phenomenon is that, for motor acceleration, the electromagnetic torque increases to about 7.8 Nm for speeding up, and then returns to 2 Nm when the speed reaches the reference. Also, all four methods are able to track the reference speed in a short time. By further careful observation, it can be seen that the proposed method shows less ripples and oscillations in stator currents during transient.

VI. HIL EXPERIMENT

In the experiment, the steady-state performance, speed transient response and load torque dynamic response of the proposed control strategy are all evaluated. The experimental setup consists of a laptop, an OPAL-RT OP5700 simulator, a DSP with F28335 chip, and an oscilloscope as shown in Fig. 7. The laptop is used to develop the proposed MPDSC code, and download it to the DSP. Apart from the MPDSC code, the rest of PMSM system is implemented using RT-LAB. The PMSM, the DC bus and the inverter are modelled and run in the OP5700 simulator. DSP gathers the machine information from the OP5700 simulation through

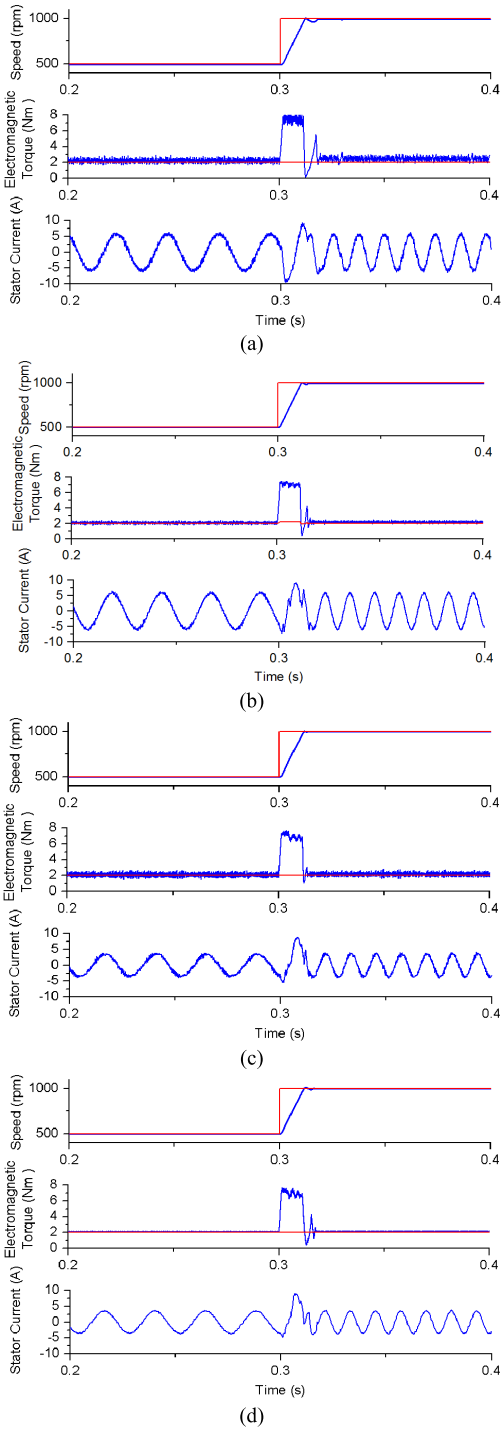

FIGURE 6. Comparisons of dynamic response for various control methods when speed changes from 500 rpm to 1000 rpm: (a) conventional DTC, (b) conventional MPDSC, (c) SCF-MPDSC, (d) proposed DCF-MPDSC.

the DSP input interface. The PWM gate driving signals, generated by the DSP, will output to the OP5700 simulator to control the PMSM.

The sampling time is set to 100 μs. The PMSM system parameters are the same as those listed in Table 3. Fig. 8 shows the stead-state performance. Fig. 9 presents a dynamic response when speed steps up from 500 rpm to 1000 rpm. The

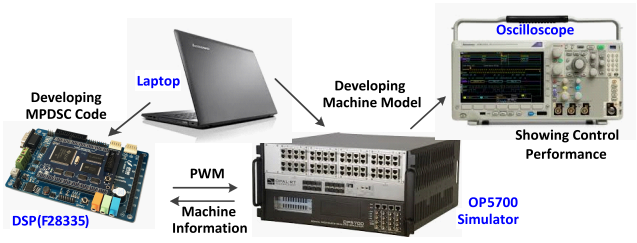

FIGURE 7. HIL testbed setup.

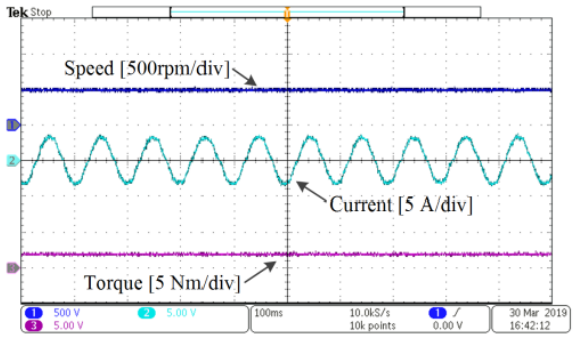

FIGURE 8. Steady state response of the proposed DCF-MPDSC strategy when speed is 500 rpm.

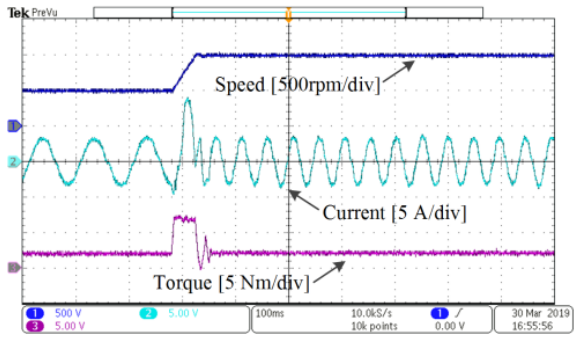

FIGURE 9. Dynamic response of the proposed DCF-MPDSC strategy when speed is changed from 500 rpm to 1000 rpm.

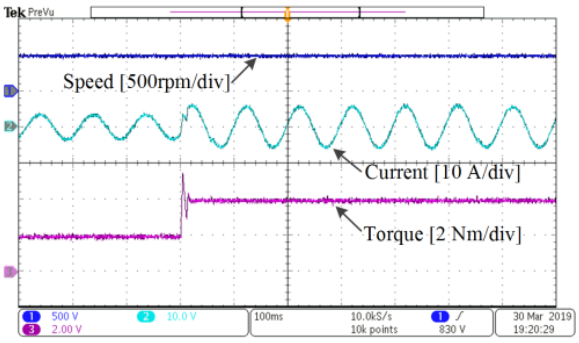

FIGURE 10. Dynamic response of the proposed DCF-MPDSC strategy when load torque is changed from 2 Nm to 4 Nm.

dynamic responses of load torque are shown in Fig. 10 with a speed change from 2 Nm to 4 Nm.

It can be seen that the motor performs with a satisfactory control performance, especially on the dynamic response of speed, i.e., very small speed offset and speed ripple. The presented results are in good agreement with the simulation, validating the effectiveness of the proposed DCF-MPDSC.

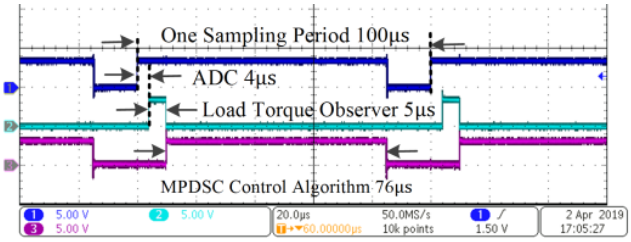

FIGURE 11. Computational time of proposed DCF-MPDSC in digital implementation.

In practical digital implementation in motor drives, the control algorithms must be executed completely in the digital signal processors within every control period. Otherwise, the system performance will be compromised. This is particularly important for control methods like predictive speed control where duty ratio calculation and system status prediction are involved. To evaluate the computational burden of the proposed strategy, the computational time for each control process is measured, as is indicated in Fig. 11. The total computational time of the entire controller is 85μs. Specifically, the completeness of ADC process requires about 4μs, and the load torque observer takes around 5μs to estimate the load torque. Then, it takes about 76μs to execute the main DCF-MPDSC algorithm. As the whole control period is 100μs, the proposed control method can execute completely. This demonstrates the feasibility of the practical implementation of the proposed method.

VII. CONCLUSION AND FUTURE WORKS

In this paper, a new DCF-MPDSC is proposed to enhance the control performance on speed offset, speed ripple and torque ripple. Eight duty ratios are integrated with eight voltage vectors to form eight combinations of voltage vectors. An optimal combination of voltage vectors is finally selected through two cost functions acting sequentially. The feasibility and superiority of the proposed DCF-MPDSC have been well validated in comprehensive comparison studies. The results prove that the proposed method has an excellent control performance with THD 4.43%, torque ripple 0.0423Nm, speed ripple 0.0121rpm, and speed offset 0.0055%, and a high potential in motor drives where accurate speed tracking ability is of high priority.

Nevertheless, the proposed DCF-MPDSC strategy relies on the machine parameters to derive and predict the future motor behaviors. Further enhancement of the system robustness against parameter variation is still ongoing. Besides, the proposed DCF-MPDSC strategy is fairly computational demanding which limits the use of high switching frequency to enhance the control performance. Further research would also focus on reducing the complexity of the proposed DCF-MPDSC strategy without deteriorating the excellent speed tracking capability.

REFERENCES

[1] S. Lu and X. Wang, "Observer-based command filtered adaptive neural network tracking control for fractional-order chaotic PMSM," *IEEE Access*, vol. 7, pp. 88777–88788, 2019.
[2] X. Zhao, X. Wang, L. Ma, and G. Zong, "Fuzzy approximation based asymptotic tracking control for a class of uncertain switched nonlinear systems," *IEEE Trans. Fuzzy Syst.*, vol. 28, no. 4, pp. 632–644, Apr. 2020.
[3] Y. Chang, Y. Wang, F. E. Alsaadi, and G. Zong, "Adaptive fuzzy output-feedback tracking control for switched stochastic pure-feedback nonlinear systems," *Int. J. Adapt. Control*, vol. 33, no. 10, pp. 1567–1582, 2019.
[4] S. Kouro, P. Cortes, R. Vargas, U. Ammann, and J. Rodriguez, "Model predictive Control—A simple and powerful method to control power converters," *IEEE Trans. Ind. Electron.*, vol. 56, no. 6, pp. 1826–1838, Jun. 2009.
[5] Y. Shan, J. Hu, Z. Li, and J. M. Guerrero, "A model predictive control for renewable energy based AC microgrids without any PID regulators," *IEEE Trans. Power Electron.*, vol. 33, no. 11, pp. 9122–9126, Nov. 2018.
[6] P. Falkowski and A. Sikorski, "Finite control set model predictive control for grid-connected AC–DC converters with LCL filter," *IEEE Trans. Ind. Electron.*, vol. 65, no. 4, pp. 2844–2852, Apr. 2018.
[7] Y. Zhang, Y. Peng, and H. Yang, "Performance improvement of Two-Vectors-Based model predictive control of PWM rectifier," *IEEE Trans. Power Electron.*, vol. 31, no. 8, pp. 6016–6030, Aug. 2016.
[8] T. Geyer, "Algebraic tuning guidelines for model predictive torque and flux control," *IEEE Trans. Ind. Appl.*, vol. 54, no. 5, pp. 4464–4475, Sep. 2018.
[9] M. H. Arshad, M. A. Abido, A. Salem, and A. H. Elsayed, "Weighting factors optimization of model predictive torque control of induction motor using NSGA-II with TOPSIS decision making," *IEEE Access*, vol. 7, pp. 177595–177606, 2019.
[10] Y. Luo and C. Liu, "Multi-Vector-Based model predictive torque control for a six-phase PMSM motor with fixed switching frequency," *IEEE Trans. Energy Convers.*, vol. 34, no. 3, pp. 1369–1379, Sep. 2019.
[11] Y. Zhou, H. Li, R. Liu, and J. Mao, "Continuous voltage vector model-free predictive current control of surface mounted permanent magnet synchronous motor," *IEEE Trans. Energy Convers.*, vol. 34, no. 2, pp. 899–908, Jun. 2019.
[12] D. Su, C. Zhang, and Y. Dong, "Finite-state model predictive current control for surface-mounted permanent magnet synchronous motors based on current locus," *IEEE Access*, vol. 5, pp. 27366–27375, 2017.
[13] Y. Zhang and H. Yang, "Model-predictive flux control of induction motor drives with switching instant optimization," *IEEE Trans. Energy Convers.*, vol. 30, no. 3, pp. 1113–1122, Sep. 2015.
[14] S. Rubino, R. Bojoi, S. A. Odhano, and P. Zanchetta, "Model predictive direct flux vector control of Multi-three-Phase induction motor drives," *IEEE Trans. Ind. Appl.*, vol. 54, no. 5, pp. 4394–4404, Sep. 2018.
[15] P. Kakosimos and H. Abu-Rub, "Deadbeat predictive control for PMSM drives with 3-L NPC inverter accounting for saturation effects," *IEEE J. Emerg. Sel. Topics Power Electron.*, vol. 6, no. 4, pp. 1671–1680, Dec. 2018.
[16] Y. Luo and C. Liu, "A simplified model predictive control for a dual three-phase PMSM with reduced harmonic currents," *IEEE Trans. Ind. Electron.*, vol. 65, no. 11, pp. 9079–9089, Nov. 2018.
[17] Y. Luo and C. Liu, "A flux constrained predictive control for a six-phase PMSM motor with lower complexity," *IEEE Trans. Ind. Electron.*, vol. 66, no. 7, pp. 5081–5093, Jul. 2019.
[18] C. Sun, D. Sun, Z. Zheng, and H. Nian, "Simplified model predictive control for dual inverter-fed open-winding permanent magnet synchronous motor," *IEEE Trans. Energy Convers.*, vol. 33, no. 4, pp. 1846–1854, Dec. 2018.
[19] Z. Zhou, C. Xia, Y. Yan, Z. Wang, and T. Shi, "Disturbances attenuation of permanent magnet synchronous motor drives using cascaded Predictive-Integral-Resonant controllers," *IEEE Trans. Power Electron.*, vol. 33, no. 2, pp. 1514–1527, Feb. 2018.
[20] M. Shao, Y. Deng, H. Li, J. Liu, and Q. Fei, "Robust speed control for permanent magnet synchronous motors using a generalized predictive controller with a high-order terminal sliding-mode observer," *IEEE Access*, vol. 7, pp. 121540–121551, 2019.
[21] R. S. Dastjerdi, M. A. Abbasian, H. Saghafi, and M. H. Vafaie, "Performance improvement of permanent-magnet synchronous motor using a new deadbeat-direct current controller," *IEEE Trans. Power Electron.*, vol. 34, no. 4, pp. 3530–3543, Apr. 2019.
[22] X. Zhang, B. Hou, and Y. Mei, "Deadbeat predictive current control of permanent-magnet synchronous motors with stator current and disturbance observer," *IEEE Trans. Power Electron.*, vol. 32, no. 5, pp. 3818–3834, May 2017.
[23] Y. Zhang, Y. Bai, and H. Yang, "A universal multiple-vector-based model predictive control of induction motor drives," *IEEE Trans. Power Electron.*, vol. 33, no. 8, pp. 6957–6969, Aug. 2018.
[24] X. Zhang and B. Hou, "Double vectors model predictive torque control without weighting factor based on voltage tracking error," *IEEE Trans. Power Electron.*, vol. 33, no. 3, pp. 2368–2380, Mar. 2018.
[25] G. Li, J. Hu, Y. Li, and J. Zhu, "An improved model predictive direct torque control strategy for reducing harmonic currents and torque ripples of five-phase permanent magnet synchronous motors," *IEEE Trans. Ind. Electron.*, vol. 66, no. 8, pp. 5820–5829, Aug. 2019.
[26] R. E. Kodumur Meesala, V. P. K. Kunisetti, and V. Kumar Thippiripati, "Enhanced predictive torque control for open end winding induction motor drive without weighting factor assignment," *IEEE Trans. Power Electron.*, vol. 34, no. 1, pp. 503–513, Jan. 2019.
[27] M. Norambuena, J. Rodriguez, Z. Zhang, F. Wang, C. Garcia, and R. Kennel, "A very simple strategy for high-quality performance of AC machines using model predictive control," *IEEE Trans. Power Electron.*, vol. 34, no. 1, pp. 794–800, Jan. 2019.
[28] M. Preindl and S. Bolognani, "Model predictive direct speed control with finite control set of PMSM drive systems," *IEEE Trans. Power Electron.*, vol. 28, no. 2, pp. 1007–1015, Feb. 2013.
[29] V. Šmídl, J. Š., L. Adam, and Z. Peroutka, "Direct speed control of a PMSM drive using SDRE and convex constrained optimization," *IEEE Trans. Ind. Electron.*, vol. 65, no. 1, pp. 532–542, Jan. 2018.
[30] P. Kakosimos and H. Abu-Rub, "Predictive speed control with short prediction horizon for permanent magnet synchronous motor drives," *IEEE Trans. Power Electron.*, vol. 33, no. 3, pp. 2740–2750, Mar. 2018.
[31] M. Liu, K. W. Chan, J. Hu, W. Xu, and J. Rodriguez, "Model predictive direct speed control with torque oscillation reduction for PMSM drives," *IEEE Trans. Ind. Informat.*, vol. 15, no. 9, pp. 4944–4956, Sep. 2019.
[32] Y. Yan, J. Yang, Z. Sun, C. Zhang, S. Li, and H. Yu, "Robust speed regulation for PMSM servo system with multiple sources of disturbances via an augmented disturbance observer," *IEEE/ASME Trans. Mechatronics*, vol. 23, no. 2, pp. 769–780, Apr. 2018.
[33] Y. Yan, J. Yang, Z. Sun, S. Li, and H. Yu, "Non-linear-disturbance-observer-enhanced MPC for motion control systems with multiple disturbances," *IET Control Theory Appl.*, vol. 14, no. 1, pp. 63–72, Jan. 2020.
[34] J. Yang, W. Chen, S. Li, L. Guo, and Y. Yan, "Disturbance/uncertainty estimation and attenuation techniques in PMSM drives—A survey," *IEEE Trans. Ind. Electron.*, vol. 64, no. 4, pp. 3273–3285, Apr. 2017.
[35] K. Ogata, *Modern Control Engineering: Control System Design in State Space*, 5th ed. London, U.K.: Pearson, 2009, ch. 10.
[36] M. Preindl and S. Bolognani, "Model predictive direct torque control with finite control set for PMSM drive systems, part 1: Maximum torque per ampere operation," *IEEE Trans. Ind. Informat.*, vol. 9, no. 4, pp. 1912–1921, Nov. 2013.
[37] I. Takahashi and T. Noguchi, "A new quick-response and high-efficiency control strategy of an induction motor," *IEEE Trans. Ind. Appl.*, vol. IA-22, no. 5, pp. 820–827, Sep. 1986.
[38] M. Depenbrock, "Direct self-control (DSC) of inverter-fed induction machine," *IEEE Trans. Power Electron.*, vol. 3, no. 4, pp. 420–429, Oct. 1988.

MING LIU received the B.Eng. degree in electrical engineering from Qingdao University, Qingdao, China, in 2014, and the Ph.D. degree in electrical engineering from The Hong Kong Polytechnic University (PolyU), Hong Kong, in 2020. He is currently a Postdoctoral Fellow with the Department of Electrical Engineering, PolyU, working on intelligent control algorithms for motor drives. His research interests include model predictive control and wireless power transfer.

JIEFENG HU (Senior Member, IEEE) received the Ph.D. degree in electrical engineering from the University of Technology Sydney (UTS), Australia, in 2013. He was involved in the research of minigrids in Commonwealth Scientific and Industrial Research Organization (CSIRO), Newcastle, NSW, Australia. He was an Assistant Professor with The Hong Kong Polytechnic University, Hong Kong. He is currently an Associate Professor and the Program Coordinator of electrical engineering with Federation University Australia. His research interests include power electronics, renewable energy, and smart microgrids. He is an Editor of the IEEE TRANSACTIONS ON ENERGY CONVERSION, an Associate Editor of *IET Renewable Power Generation*, and a Guest Editor of the IEEE TRANSACTIONS ON INDUSTRIAL ELECTRONICS.

KA WING CHAN (Member, IEEE) received the B.Sc. (Hons.) and Ph.D. degrees in electronic and electrical engineering from the University of Bath, U.K., in 1988 and 1992, respectively. He is currently an Associate Professor and an Associate Head of the Department of Electrical Engineering, The Hong Kong Polytechnic University. His research interests include power system stability, analysis and control, power grid integration, security, resilience and optimization, demand response management, and so on.

SIU WING OR received the B.Sc. (Hons.), M.Phil., and Ph.D. degrees in engineering physics from The Hong Kong Polytechnic University (PolyU), Hong Kong, in 1995, 1997, and 2001, respectively. From 1995 to 2001, he was a Teaching Company Associate, a Research Electronic Engineer, and a Senior Research Electronic Engineer with ASM Pacific Technology Ltd., Hong Kong. He was a Postdoctoral Research Fellow with the Mechanical and Aerospace Engineering Department, University of California at Los Angeles, Los Angeles, CA, USA, for a period of one and a half years, before he joined PolyU, as a Lecturer, in 2002. He is currently a Professor, the Director of the Smart Materials and Systems Laboratory, and the Director of the Electrical Protection and High Voltage Coordination Laboratory, Department of Electrical Engineering, PolyU. He has authored or coauthored more than 300 publications, including two professional book chapters, more than 200 SCI journal articles, and more than 100 international conference papers. He holds 43 patents. His research interests include smart materials and devices in the bulk, micro, and nanoscale, electrical condition monitoring, electromagnetic absorption and shielding, and energy harvesting, storage, and management.

SIU LAU HO received the B.Sc. and Ph.D. degrees in electrical engineering from the University of Warwick, Coventry, U.K., in 1976 and 1979, respectively. Since 1979, he has been with the Department of Electrical Engineering, The Hong Kong Polytechnic University, Hong Kong, where he is currently an Associate Vice President (Academic Support) cum Registrar and the Chair Professor of electricity utilization. He has authored or coauthored more than 350 articles in SCI journals, mostly in the IEEE TRANSACTIONS and the *Institute of Engineering and Technology Proceedings*, more than 300 international conference papers, and holds several patents. His research interests include condition monitoring of railway systems, novel sensors, optimization of electromagnetic devices, phantom loading of electrical machines, and design and development of novel machines. He is a member of the Hong Kong Institution of Engineers.

WENZHENG XU received the B.Eng. degree in electrical engineering from Beijing Jiaotong University, Beijing, China, in 2012, the M.Sc. degree (Hons.) from The University of Hong Kong, Hong Kong, in 2013, and the Ph.D. degree in electrical engineering from The Hong Kong Polytechnic University (PolyU), Hong Kong, in 2020. From September 2013 to June 2015, he was a Research Assistant with the Department of Electrical Engineering, PolyU. He is currently a Postdoctoral Fellow with the Department of Electrical Engineering, PolyU, working on high-power converters and fast-charging devices for electric vehicles. His research interests include power electronics topologies, dual-active-bridge converters, bi-directional dc-ac converters, wireless power transfer, and their applications in transportation electrification.

XIAN ZHANG (Member, IEEE) received the B.Sc. degree in electrical engineering from North China Electric Power University, Beijing, China, in 2009, the M.Sc. degree in electrical engineering from Tsinghua University, Beijing, in 2012, and the Ph.D. degree in electrical engineering from The Hong Kong Polytechnic University (PolyU), Hong Kong, in 2019. Since 2019, she has been a Postdoctoral Fellow with the Department of Electrical Engineering, PolyU, working in fields of smart grid and electric vehicles planning.